Journal of MATERIALS RESEARCH

Article
DOI:10.1557/s43578-022-00541-1

# Accurate measurement of thin film mechanical properties using nanoindentation

S. Zak[1,a], C. O. W. Trost[1], P. Kreiml[1], M. J. Cordill[1,2]

[1] Erich Schmid Institute of Materials Science, Austrian Academy of Sciences, Jahnstraße 12, 8700 Leoben, Austria
[2] Department of Materials Science, Montanuniversität Leoben, Jahnstraße 12, 8700 Leoben, Austria
[a)] Address all correspondence to this author. e-mail: stanislav.zak@oeaw.ac.at

Received: 8 November 2021; accepted: 14 March 2022; published online: 1 April 2022

**For decades, nanoindentation has been used for measuring mechanical properties of films with the widely used assumption that if the indentation depth does not exceed 10% of the film thickness, the substrate influence is negligible. The 10% rule was originally deduced for much thicker metallic films on steel substrates and involved only the hardness measurement. Thus, the boundaries of usability for measuring thin film elastic modulus may differ. Two known material systems of Mo and MoTa thin films on Si substrates are examined with nanoindentation and numerical modeling to show the limitations in measuring elastic moduli. An assessment of the hardness and elastic modulus as a function of contact depth and accurate modeling of the film/substrate deformation confirms the 10% rule for hardness measurements. For elastic modulus, the indentation depths should be much smaller. Results provide a recommended testing protocol for accurate assessment of thin film elastic modulus using nanoindentation.**

## Introduction

Since its introduction to the field of materials science, nanoindentation became an integral technique to evaluate the mechanical behavior of a variety of materials. One area, where nanoindentation was found to be particularly useful, was with thin films [1]. Nanoindentation is the simplest method to measure hardness, and in some cases, elastic modulus. In order to work around the influence of the substrate, the 10% rule of thumb, first introduced by Bückle [2] in 1953, is applied. The general definition of the 10% rule of thumb is that the mechanical properties of a film, hardness and elastic modulus, can be measured when indents are made to 10% or less of the film thickness. In practice, however, only indenting 10% of the film thickness is not practical for ultra-thin films (< 10 nm) or even thin films (20 nm–1 μm) and the behavior would still be somewhat dependent on the substrate (hard, rigid substrate vs. soft, compliant substrate). Other problems could also arise from the well-known indentation size effect (ISE), tip area function calibrations, or even the sharpness of the used tip. It is important to be able to measure the hardness, which is often used as the basis for evaluation of the yield stress of many materials [3, 4], and a reliable value of the elastic modulus so that simulations, modeling and additional subsequent calculations have the correct material input.

The 10% rule of thumb has been accepted in the experimental community and taught within the field without robust validation and very little theoretical understanding behind it. Thus, many authors have used the 10% rule of thumb to measure hardness and elastic modulus without understanding its origins. In the original paper by Bückle, the 10% rule of thumb comes from micro-indents performed on an 8 μm thick hard coating on a steel substrate (hard on soft system). Only hardness was discussed and elastic modulus is never measured. Bückle states [2], "It is found that for a hard coating on less hard substrates the intrinsic hardness of the coating is measured with indentation the depth of which are less than a tenth of the coat thickness." What is important about Bückle's statement is that it is, (1) qualified for hard coatings on less hard substrates and (2) only for hardness. With time, the 10% rule of thumb has evolved to include elastic modulus, which was never discussed in the original paper. However, Xu and Rowcliffe [5] found that "… there is no universal critical penetration depth for measuring the mechanical properties of films. The critical penetration depth depends on the combination of the mechanical properties of the

film/substrate system." Newer insight from Bull [6] found that while hardness can be measured using 10% of the film thickness, the elastic modulus should only be considered at much lower indentation depths being less than 1% of the film thickness.

Over the years, new methods and models have been developed to measure film-only hardness [7–10] and elastic modulus [6, 9–12]. For example, Saha and Nix [10, 13] introduced a constant modulus idea first employed by Joslin and Oliver (J–O) [14]. In this case, dynamic indentation is necessary and the $P^2/S$, where $P$ is the indentation load and $S$ the stiffness, is proportional to hardness. One can then measure the hardness, $H$, for a film on a stiffer substrate or the same substrate as the film and then use that $H$ as feedback to calculate the elastic modulus, $E$, of the film in question. This model can work because it also removes pile-up effects, but it assumes the same microstructure (grain size and texture) of the indented material for comparable results, however, this may not be the case for the different substrates. Due to surface energy differences, a constant microstructure should not always be assumed for any film-substrate combination, thus the hardness measured may not be the same for the different substrates. Nix [15, 16] used the standard relation by Sneddon [17] for the elastic and plastic solution for thin film nanoindentation, however, this research is aimed more in the direction of hardness measurements and dislocation strengthening for use with film thicknesses in range of several micrometers. Furthermore, Saha et al. [18] investigates strain gradient hardening effects with use of soft film on hard substrate system, showing the dependence of the measured E and H on the indentation depth even though the used material combination favors the film deformation during the nanoindentation. An additional model by Li and Vlassak [12] uses Yu's solution [19] for the elastic contact of an indenter instead of Sneddon's solution [17]. The model can be applied to thin films and ultra-thin films over a large indentation depth, but it is again best to use dynamic indentation or have many data points (100 or more). The model is only ideal for single films and not multilayers. Still, a straightforward assessment of the thin film elastic modulus is to indent to various depths and plot the measured $E$ as a function of contact depth, $h_c$, or contact depth over film thickness ($h_c/t$). The film modulus is then found by extrapolating the curve of the best fit data to zero [20]. While this approach can lead to a value for $E$, it may not be realistic or correct, and is quite subjective to what one considers to be the "best" fit.

It should be noted that not all nanoindenters are equipped with dynamic indentation (also known as the continuous stiffness method), which many of the newer models utilize to extract $H$ and $E$ [10, 12, 13, 21]. The benefit of dynamic indentation (with an oscillation during loading) over quasi-static indentation (no oscillation during loading) is minimal. Different groups have observed that in single crystals or large grained bulk materials dynamic indentation measured lower hardness values [22–24]. More recently it was determined that some of the dynamic softening effect of the measured hardness is caused by the material being strain rate sensitive [25]. For thin films, some softening effects have been observed for single crystal Ni films (20 and 100 nm thick) on MgO and the behavior was described with molecular dynamics simulations [26, 27]. In general, one could say that the indentation method does not play a significant role unless the material is strain rate sensitive and other parameters, including tip radius need to be considered. For more extensive studies finite element (FE) modeling is often used as an efficient and effective way to study tip shape effects [28]. Finally, ISE could also influence the measurement of film-only mechanical behavior, especially hardness. ISE is observed as an increase in the hardness as the contact depth of the indent decreases (reaches the surface). It has also been studied for bulk [29–34] and thin film indentation [26, 27, 35]. The effects from ISE can be easily removed from the real behavior when many indents are performed near the surface, approximately 1–5% of the film thickness.

A question that hopefully arises is, how can hardness and elastic modulus be measured for thin films accurately and independent of the substrate? First, consider the elastic and plastic zones that are created under an indenter. Bull [6] has described these two regimes as short range and long range (Fig. 1), where hardness is a short range property and elastic modulus is a long range property. In order to measure film-only hardness, the plastic zone under the indent should remain in the film. A similar argument can be made for the elastic modulus of a thin film, however, the elastic zone can be at least three times larger than the plastic zone [3, 6]. With the elastic zone being so much larger than the plastic zone, indenting to acceptable depths while maintaining good tip characteristics (a well-calibrated tip at very low indentation depth) is a challenge. Applying the concept of short- and long range properties to a thin film system would provide some physical means to how film-only properties could be measured and to the validity of using the 10% rule of thumb.

The measured values of elastic moduli and hardness are the direct response of the elastic and plastic zones (volumes) in the indented material, in our case in a thin film. Besides

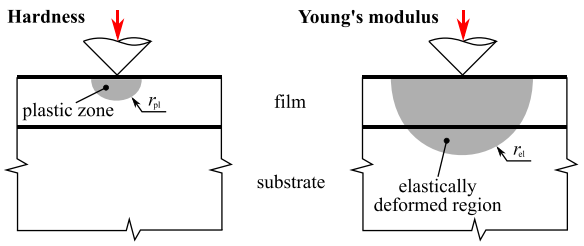


**Figure 1:** Schematic of the difference between plastic deformation (hardness measurement) and elastic deformation (Young's modulus measurement) under the indenter according to Bull [6].

some special methods, such as photo-elasticity [36–38] or digital image correlation (DIC) [39–41] which are not usable for direct measurement of the stress–strain fields inside the bulk of a material on the micro-scale level, there is no straightforward experimental way to obtain the extent of elastic and/or plastic zone under the nanoindenter. Advanced in situ nanodiffraction methods have been developed and used to measure the stresses occurring under the indenter of thick hard coatings [42]. This method is powerful, but inefficient as a method to simply measure hardness or elastic modulus due to the intricate sample preparation, small microstructures, need for synchrotron beam line to perform the experiment, and extensive data analysis. To understand how the deformation evolves with increasing indentation depth, numerical modeling, such as finite element (FE) analysis, represents an ideal tool to be used. While there are numerous works related to FE modeling of indentation processes (e.g. [11, 28, 43–49]), they are mainly aimed at the investigation and modeling of plasticity-related phenomena, surface roughness influences and hardness measurements. Only a few FE modeling studies have been performed with the aim to calculate the critical ratio of coating thickness to indentation depth (CRTD) [5, 50, 51] by the deviation of the load–displacement curve from the bulk load–displacement curve. By defining the CRTDs over the elastic and plastic fields for the hardness and elastic modulus, respectively, the definition not only becomes more physically grounded, there is also no need to decide which amount of deviation of the curve is considered reasonable. A proper analysis of elastic field under the indenter tip has been vastly neglected, even though the FE modeling methods are well-suited for the evaluation of very small elastic deformations. Therefore, the knowledge of the size and shape of both elastic and plastic zones in the thin film during the indentation and their comparison (from the FE models) can be a significant advancement for understanding the elastic moduli measurements by nanoindentation and with it, the applicability of the 10% rule can be tested and verified under several different conditions, which is the main goal of this work.

It should be noted that an optional method for precise measurement of thin film mechanical properties can be cross-sectional nanoindentation. This method can be performed similarly to characterization of the adhesion of thin films by cross-sectional nanoindentation (as reported in [52]), only with much smaller loading force or depth and with the indents precisely placed in the area of the film cross-section (CS). Such method would fully circumvent the 10% rule by indenting in the direction where there is no presence of the substrate. However, the positioning of such indents may be difficult and the lateral sample deformation may lead to distorted results. Therefore, the cross-sectional nanoindentation was performed within this research next to standard nanoindentation to compare the obtained results.

## Results and discussion

### Experiments

As a direct result from nanoindentation the load–displacement ($P$–$\delta$) curves were extracted. $P$–$\delta$ curves exhibit expected behavior for all examined cases. The indentation with the lowest load shows linear, elastic material behavior, but with increasing load plastic deformation starts to play a significant role. The maximum depth of all indents remained in the films studied, namely 1 and 2 μm thick Mo and MoTa films on Si, with none of the indents reaching the interface between the film and substrate.

The indentation $P$–$\delta$ curves were subjected to evaluation of hardness, $H$, and Young's modulus, $E$, with Oliver–Pharr (O–P) [53] and Joslin-Oliver (J–O) [14] methods. The resulting $H$ and $E$ values are shown in Fig. 2 for both Mo and MoTa films as a function of contact depth over film thickness ($h_c/t$) in %. All data points are shown to illustrate how indentation methods need many indents to bring about statistically relevant results. Relying on only 10 indents to measure the mechanical behavior would be an error. The indentation results for the Si substrate show consistent values of both $H$ and $E$ across the whole range of $h_c/t$, resulting in $E_{Si} = 173 \pm 5.4$ GPa and $H_{Si} = 12.2 \pm 0.45$ GPa. For the evaluation of the mean value and the standard deviation for Si, the indentation results for $h_c/t > 0.05$ were used, since the scattered data for lower contact depths are clearly influenced by numerous insignificant errors, which if combined together causes a large uncertainty of very shallow indents. These errors may be caused by small uncertainties in the tip calibration function, blunting of the tip during the indentation, the sample surface roughness and ISE in case of hardness measurement. Therefore, results for Si with $h_c/t < 0.05$ do not represent correct values. Measured hardness and elastic modulus of the Si is in a good agreement with well-known Si material properties (see, e.g. [54–57]), the standard deviation is in acceptable range and the obtained data are independent of the contact depth, since the substrate is thick enough to behave like a bulk material. In the case of either Mo or MoTa alloy thin films a distinct dependence of the $E$ and $H$ on the contact depth is clearly visible. Since the influence is different for $H$ and $E$, these material properties will be discussed separately.

***Hardness Zones:*** Both film thicknesses and films show similar trends of the dependence of $H$ on $h_c/t$ and as is clearly visible in Fig. 2(a) and (b), the datasets can be divided into three separate zones. Note that these results are only valid for this materials system and should not be (mis-)used as a new rule of thumb without precise characterization of the system:

*H1—surface zone*: for $h_c/t < 2.5\%$ of the film thickness, the hardness values are scattered and they may be shifted to lower values. In this region there is no possibility to obtain a precise value of the $H$. This is caused mainly by three factors. First, hardness is related to the plastic deformation of the

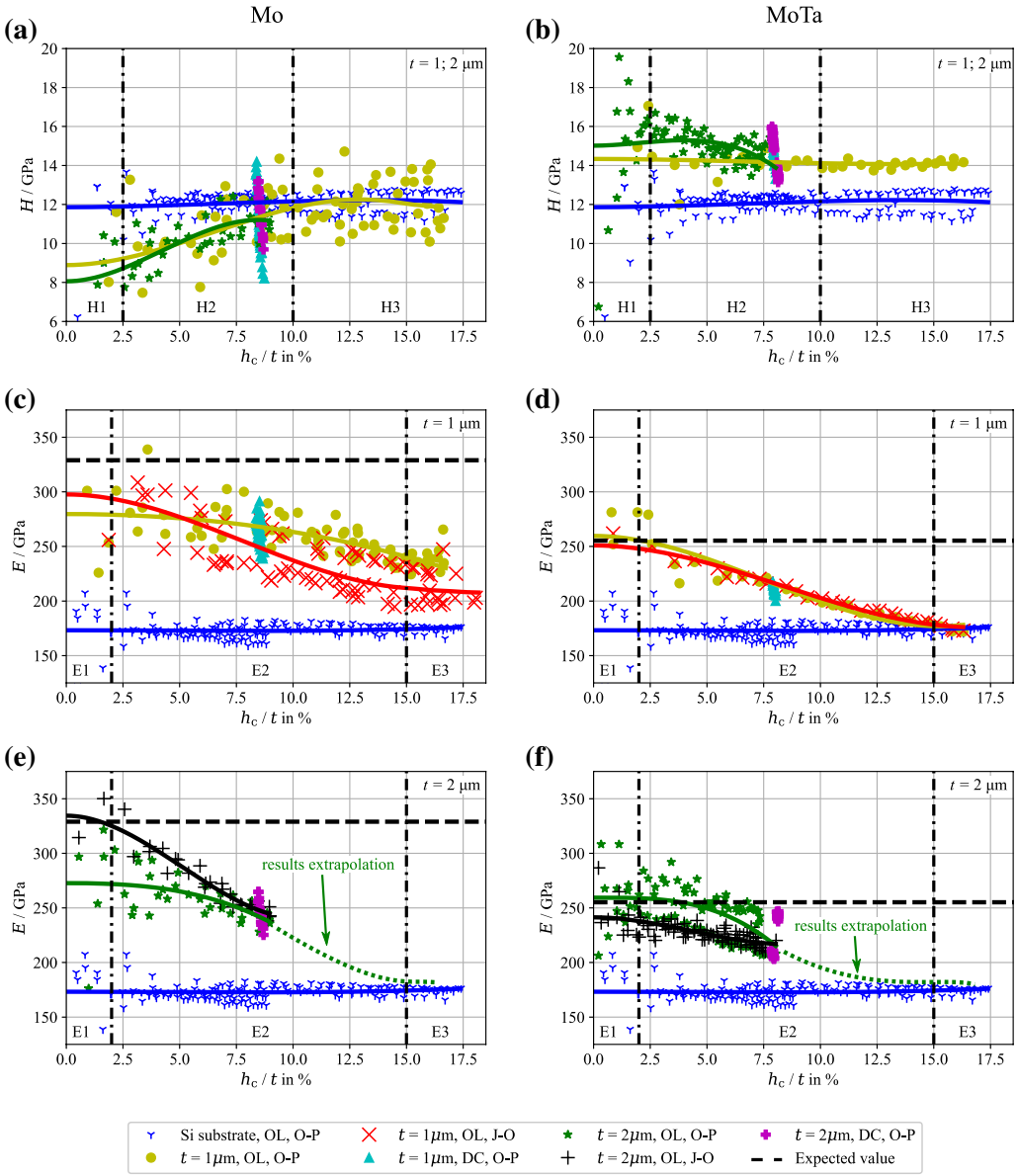


**Figure 2:** Experimentally measured Young's modulus, *E*, and hardness, *H*, as a function of the contact depth, $h_c$, normalized to film thickness, *t* (for the Si substrate indentation the normalization was performed according to the thickness of the deposited film on the measured Si samples), from open loop (OL) and displacement control (DC) indents; left column is for Mo films, right column for MoTa films: (a) and (b) is for *H*, (c) and (d) is for *E* and film thickness 1 µm, (e) and (f) is for *E* and film thickness 2 µm; dash-dotted lines represents the boundaries between the specific zones H1, H2 and H3 for hardness measurements and E1, E2 and E3 for Young's modulus measurement (for more detailed information see text).

indented material and since for low indentation depths the plastic zone under the indenter tip is virtually non-existent, the hardness cannot be defined. Secondly, the tip calibration function (tip area function) is usually difficult to properly define for small indentation depths, when measured with traditional methods. And the last influence is the roughness of the film surface, which is more pronounced for the Mo films (RMS-roughness is an order of magnitude larger for Mo film, compared to MoTa film, see "Methods" section). With large surface roughness the measured hardness values are lower. It should be noted that the decrease in hardness in this zone is not related to an ISE because the values would increase instead of decrease closer to the surface. However, this is the region where ISE would occur if all other factors would be in an ideal state.

*H2—transition zone* for $h_c/t$ in the range of 2.5% and 10% of the film thickness, the plastic zone under the indenter tip is starting to be more pronounced and the surface effects (related to roughness and the tip area function) are starting to be diminished. Therefore, there is a smooth transition to the third zone.

*H3—plateau zone* for $h_c/t > 10\%$ of the film thickness, the indentation data has a uniform progression, not dependent on the contact depth. While the end of this trend was not observed during the performed experiments, it can be deduced that the indentation up to 17.5% of the film thickness is safe for the evaluation of the film hardness for these thin film systems.

From Zone H3, the hardness for both thin films was obtained resulting in $H_{Mo} = 11.8 \pm 1.33$ GPa and $H_{MoTa} = 14.1 \pm 0.17$ GPa, which are reasonable for the materials and microstructures (seen in Fig. 8).

***Elastic Modulus Zones:*** For the measurement of the *E*, both film materials and film thicknesses exhibit a strong dependence on the contact depth. This can be easily compared with the aforementioned "10% rule of thumb" and also with known value for Mo which should have the elastic modulus of 329 GPa [58] and estimation for MoTa (using the ratio between Mo and Ta in MoTa alloy) 255 GPa. Moreover, two methods of the results evaluation can be compared (O–P and J–O). Both methods show similar trends, leading to the division of the results into three zones. Again, note that these results are only valid for these thin film systems and should not be (mis-)used as a new rule of thumb without precise characterization the system:

*E1—film-affected zone* for $h_c/t < 2\%$ of the film thickness, the resulting Young's moduli seem to converge close to the theoretical (expected) values (when $h_c/t = 0$), which is largely different than indents up to 10% of the film thickness. Therefore, only a very small portion of the film should be indented to obtain a more accurate value of the film *E*. As shown in Fig. 2(c), (d), (e) and (f), low indentation depths of 1–2% of the film thickness (approx. 10–20 nm of studied films) are vastly influenced by other factors. In a similar way as for hardness, the film surface roughness and the tip area function (tip calibration) play significant roles in the *E* measurement. The surface roughness influence is clearly visible in the results of the Mo films [Fig. 2(c) and (e)] where the roughness was significantly larger (approximately 20 nm for Mo films compared to 3 nm for the MoTa films) causing an underestimation of the *E* by indenting the rougher surface. On the other hand, a slight uncertainty of the tip calibration function for small indentation depths causes the scatter of the results which is clearly visible on both materials. The tip calibration issue can be partially resolved by the use of J–O method, leading to a smaller scatter of the results. However, while decreasing the scatter, the J–O results exhibit different behavior for the two film materials. This may be caused by the film surface roughness which was the only difference between the two films (topologically). The high roughness of the Mo thin film will introduce additional errors into the shallow indents (leading to errors in both O–P and J–O methods), therefore, the J–O method shows significant change of the *E* value for Mo film, but results comparable with O–P method for MoTa film (with low roughness).

*E2—transition zone* for $h_c/t$ between 2 and 15% of the film thickness, in this region, contrary to the widely used "10% rule of thumb", the indents are strongly influenced by the substrate. With increasing indentation depth, the measured values approach the substrate $E_{Si}$. While the scatter is considerably smaller in this region (due to the improved tip calibration at these depths), only indenting in the area of $h_c/t = 10\%$ would lead to severe underestimation of both $E_{Mo}$ and $E_{MoTa}$, measuring literally a mean value between the film and substrate [Fig. 2(c), (d), (e) and (f)].

*E3—substrate-dominated zone* $h_c/t > 15\%$ of the film thickness, both film and substrate are fully elastically deformed (and the film may exhibit full plastic deformation), therefore only the substrate plays an effective role in the material response. While it is not visible from the presented results of 2 μm thick films, an extrapolation of obtained results can be used [Fig. 2(e) and (f)] indicated by a green dotted line), proving the substrate effect. Higher loads are required to reach and surpass the interface.

It is clear that for measurements of the elastic moduli of thin films, significantly smaller indentation depths should be used (being in the Zone E1). However, it is not an easy feat to achieve an accurate measurement for indentation depths below 2% of the film thickness even for 1 and 2 μm thick films. In order to obtain the *E*-values for comparison with the known values, the extrapolation to $h_c/t = 0$ with the use of a polynomial fit [see Fig. 2(c), (d), (e) and (f)] was performed leading to values of elastic moduli $E_{Mo,\,O-P} = 276$ GPa, $E_{Mo,J-O} = 316$ GPa, $E_{MoTa,O-P} = 260$ GPa and $E_{MoTa,J-O} = 246$ GPa. While both methods for MoTa film and J–O method for Mo film are fairly close to the expected values (mainly due to the fact that J–O approach removes the roughness effect using the hardness value from larger indentation depths), the used approach and scatter in the data create large uncertainty of these results. Moreover, the depth controlled (DC) indents performed to a maximum indentation depth equal to $0.1t$ (leading to $h_c/t \sim 0.08$ at the region originally assumed by the "10% rule of thumb"), obtains the *E* value for Mo $257 \pm 14.3$ GPa and for MoTa $222 \pm 16.8$ GPa. While in a good agreement with the OL indents on the same level of $h_c$, these DC values strongly underestimate the real Young's moduli of involved materials (the same way as OL indents for similar $h_c$). It should be mentioned that the observed behavior and defined zones for the Mo and MoTa films on Si could be far from the behavior of more ductile films on rigid substrates (soft on hard systems). Future investigations are planned to study ductile film systems and this paper focuses on the Mo and MoTa film systems (hard on soft systems).

Additionally, CS indents were preformed and evaluated to eliminate the film thickness factor. Figure 3 illustrates that even shallow indents in the CS of the thin film cannot obtain the real *E* and *H* values for the Mo and MoTa, while the Si and surrounding resin measurements show expected values for *E* and *H* (for

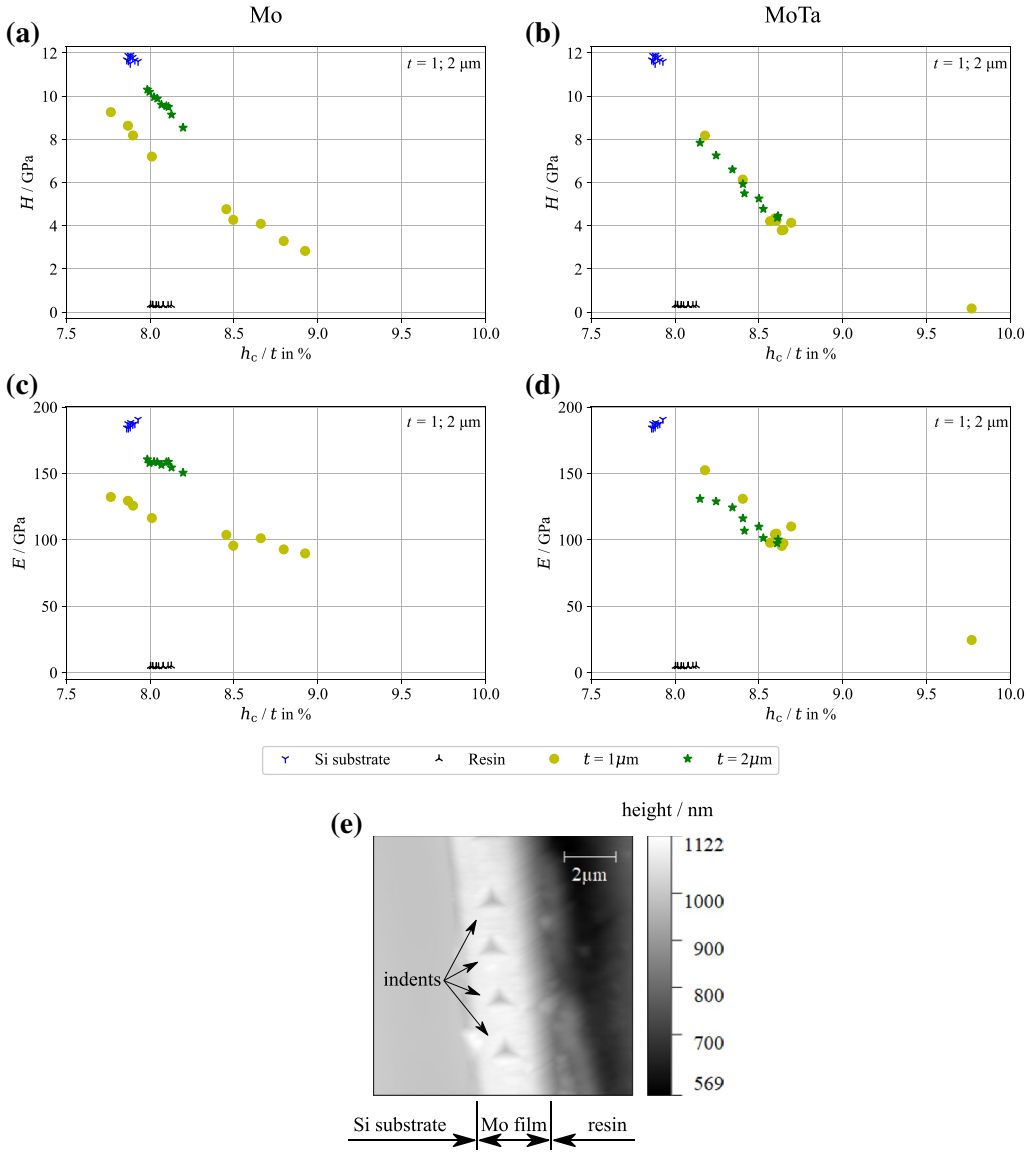


**Figure 3:** Experimentally measured Young's modulus, *E*, and hardness, *H*, as a function of the contact depth, $h_c$, normalized to film thickness, *t* (for normalization was performed according to the thickness of the deposited film on the measured samples for a better comparison with standard indents), for the sample cross-sections; left column is for Mo thin film, right column for MoTa thin film (a) and (b) is for *H*, (c), (d) is for *E* and (e) example of the tip-scanned image (height) of the CS indents in 2 µm thick Mo film.

the Si substrate, similar values as from surface indentation were obtained and for the resin, low values of $E = 4.56 \pm 0.18$ GPa and $H = 0.31 \pm 0.01$ GPa). Obviously erroneous results for Mo and MoTa CS indents were measured even though the position of the indents in the film was confirmed by imaging after the indents were made [Fig. 3(e)], ruling out the possibility of indents in the wrong position.

The measured values *E* and *H* are significantly below the expected values (less than Si substrate) for Mo and MoTa during the CS measurement illustrating an insufficient stiffness of the embedding resin. A large deformation of the resin leads to incorrect measurements. Moreover, the Mo thin film results show some dependency on the film thickness. This can be attributed to the high Mo surface roughness. Even when the CS indent is positioned at the center of the film thickness, the side related to the film surface will be less stiff with higher roughness. This is more pronounced for thinner film, since the central CS indent position is closer to the rough portion of the film, therefore, leading to lower *H* and *E* results. Because of these effects, the usual process of embedding samples in the compliant resin is not suitable for cross-sectional nanoindentation of such thin films. These results are also important for any CS indentation of foils or thicker films to obtain mechanical properties.

## Numerical Model

To explain such a large dependence of the $E$ and small dependence of the $H$ on the $h_c/t$ for surface indentation and to visualize the resin deformation during the CS indentation one has to know the exact elastically and plastically deformed volume of the material under the indenter. Since there is no easy option to measure such deformation directly, the numerical FE model was employed to estimate the influence of elastic and plastic deformation.

Several different results were extracted from the numerical simulation. At first, the basic load–displacement curves (of the indenter tip) were obtained to verify the correct model behavior. As shown in Fig. 4, the load–displacement curves obtained with numerical models are in a very good agreement with the experimental data for both Mo and MoTa films, hence the used model (geometry, boundary conditions and material properties) can be deemed appropriate for modeling nanoindentation of Mo and MoTa thin films in the region of interest. The small dissimilarities (mainly in the low force region of the unloading curve) can be attributed to the material model simplification (use of elastic—ideally plastic material model) and the idealization of the geometry of both tip and film surface. Ideal plastic material model can be considered reasonable, [5] showed that the critical penetration depth is more dependent on the difference in elastic than the plastic properties, even as the yield stress that was used as the most important parameter in [50, 51]. However, the whole unloading part of the $P$–$\delta$ curve from the FE model can be deemed only as a supportive sign of the correctness of the model, since the main objective of the numerical simulation is to assess the extent of elastically and plastically deformed zones during the indentation up to the maximal load. In that regard, the unloading parts of the $P$–$\delta$ curves from the FE model show expected behavior with an acceptable agreement with the experimental measurements. On the other hand, the loading portion of the $P$–$\delta$ curves from the FE model are much more similar to the experimental data and in this region, the FE model reproduces the real data very well. It should be noted that further improvement of the model would lead to time-consuming simulations of numerous iterations of small changes in the model geometry and material properties with no guaranteed improvements of the results. Therefore, the general agreement between presented FE model results and experimental measurement is deemed to be sufficient in the terms of this work.

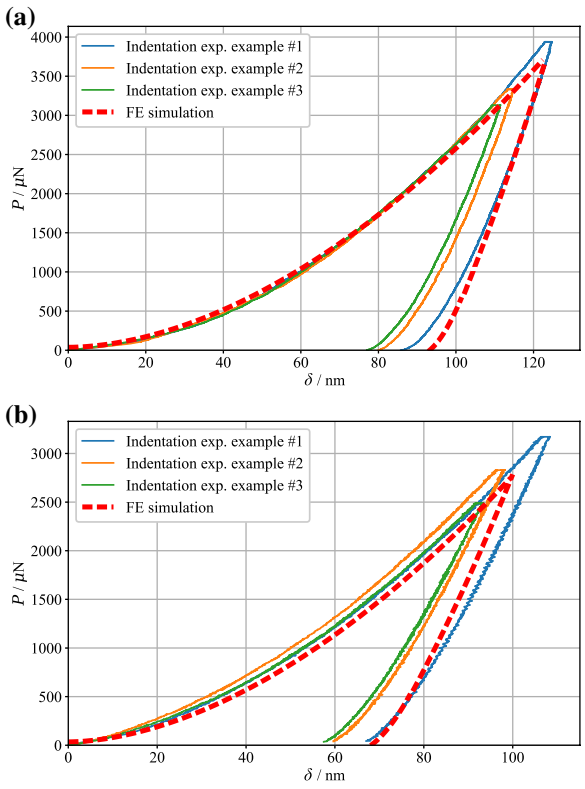


**Figure 4:** Comparison of $P$–$\delta$ curves obtained experimentally and from FE model: (a) Mo thin film, $t = 1$ μm, OL and (b) MoTa thin film, $t = 1$ μm, OL.

To evaluate the extent of elastic and plastic deformation under the indenter tip, the elastically and plastically deformed volume of the material under the tip was extracted and its major dimension, $d$ (in the direction of the indentation, see Fig. 5), was evaluated. A threshold value defining the boundary of the influenced area had to be selected. As a threshold for plastically deformed volume, the value of 0.002 of plastic strain was used (according to well-known offset yield point, where the yield limit is evaluated at the point with 0.2% of plastic strain) and for an elastically deformed volume, the value of elastic strain in the direction of indentation at $5 \times 10^{-5}$ was selected (representing approximately 16 MPa of stress in the Mo material and 13 MPa stress in the MoTa material with the approximate assumption that the stress above 10–15 MPa in any material is high enough to be noticeable) the elastic strain was used instead of the stress since it is not dependent on the elastic modulus and for the plastically deformed volume the deformation was used as well. For each step of the simulation (different indentation depths), the maximal distance of each threshold boundary, $d$ (stress/strain iso-surface), from the surface of the thin film (see Fig. 5) was obtained and plotted in a graph as a function of the indentation depth (both variables were normalized to the respective thickness of the thin film). The results from the FE model can be complemented by the estimated plastic zone radius, $r_{pl}$, evaluated from experimental measurements by formula [29, 30]:

$$r_{\mathrm{pl}} = \sqrt{\frac{3P}{2\pi \cdot \sigma_y}}, \tag{1}$$

where $P$ is the indentation load and $\sigma_y$ is the yield stress determined from the measured hardness and the well-known Tabor relation ($\sigma_y = 2.8^{*}H$).

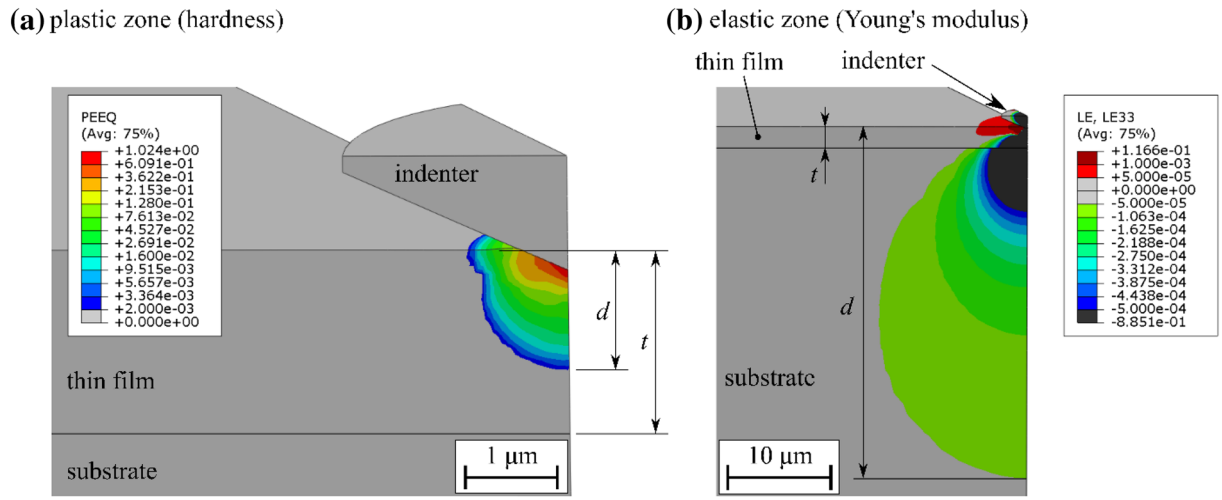


**Figure 5:** Example of the method to obtain the elastically and plastically influenced volume of the material under the indenter tip; 2 μm Mo film with indentation depth of 250 nm: a) equivalent (von-Mises) plastic strain (PEEQ) with boundary at a level of 0.002 (logarithmic scale), b) elastic strain in the direction of indentation with boundaries set to $\pm 5 \times 10^{-5}$ to highlight area with assumed non-negligible elastic deformation (colored areas).

From illustrative (but representative) Fig. 5 and from more detailed analysis in Fig. 6 one can clearly see that there is a significant difference between the sizes of elastic and plastic zones (in case of both film thicknesses and materials). Figure 5 captures the indentation process with the indentation depth only slightly larger than 10% of the film thickness (leading to final contact depth at 10% of the film thickness), but even for such a shallow indentation, the difference between short and long range (see Fig. 1 and work of Bull [6]) are clear. While the plastic zone in Fig. 5(a) is localized in the thin film, the elastically deformed zone in Fig. 5(b) extents largely into the substrate (in fact more than 15 times deeper than the film thickness, notice the different length-scales in the figure). The color spectrum in Fig. 5(b) distinguishes the severe, significant and non-negligible elastic deformation—the grey area represents negligible elastic deformation between $\pm 5 \times 10^{-5}$, the colored area highlighted in green–blue tones represents significant compressive elastic deformation and the red and black areas represent severe elastic deformation in tension and compression, respectively. One can easily see that the majority of deformed area is under compressive strain, whereas high strain values are present in the substrate. The black area, representing strains larger than $5 \times 10^{-4}$, signifies large elastic deformation of the substrate in a much greater volume, than one with the elastic deformation in the film. Therefore, the thin film only effectively bends into the deformed substrate. Moreover, it can be argued that the estimation of the elastic zone radius in [3] (approximately three times larger than the plastic zone) is largely underestimated and can represent only severe elastic deformation zones, while the actual elastic deformation spans much deeper into the substrate. These findings are furthermore confirmed by more in-depth analysis in Fig. 6. When the ratio $d/t$ reaches a value of 1 the respective strain field (its threshold value) meets the interface between the substrate and the film. The normalized plastic zone evolution under the indenter tip is similar for both film thicknesses. The plastic zone increases in both cases gradually (as expected) and it reaches the full thickness of the Mo thin film at the indentation depth of approximately 18% of the film thickness and the full thickness of the MoTa thin film at approximately 21.5% of the film thickness. A slightly higher value for MoTa film material can be expected due to its higher yield stress (or hardness). Moreover, the estimation of the plastic zone radius by Eq. (1) is in a very good agreement with numerical results, proving the validity of the FE model and showing that for hardness measurements, experiments performed with indentation depths below 20% of the film thickness can measure the actual film hardness and there is no substrate influence (for metallic thin films on a rigid substrate [5, 50, 51]). Therefore, the rule of 10% of film thickness is actually rather conservative for hardness measurements (while the experimental data are subjected to thorough investigation to exclude, e.g. roughness effects, etc.). On the other hand, the elastic zone growth in the film is extremely fast, showing that the difference between the indentation depths when the elastic or plastic zone reaches the interface between film and substrate is larger than an order of magnitude. Considerably shallow indents had to be modeled to capture the elastic zone volumetric increase in the film and the resulting data show that even indentation depths between 0.1 and 1% of the film thickness lead to noticeable elastic deformation at the film-substrate interface, illustrating the vast difference

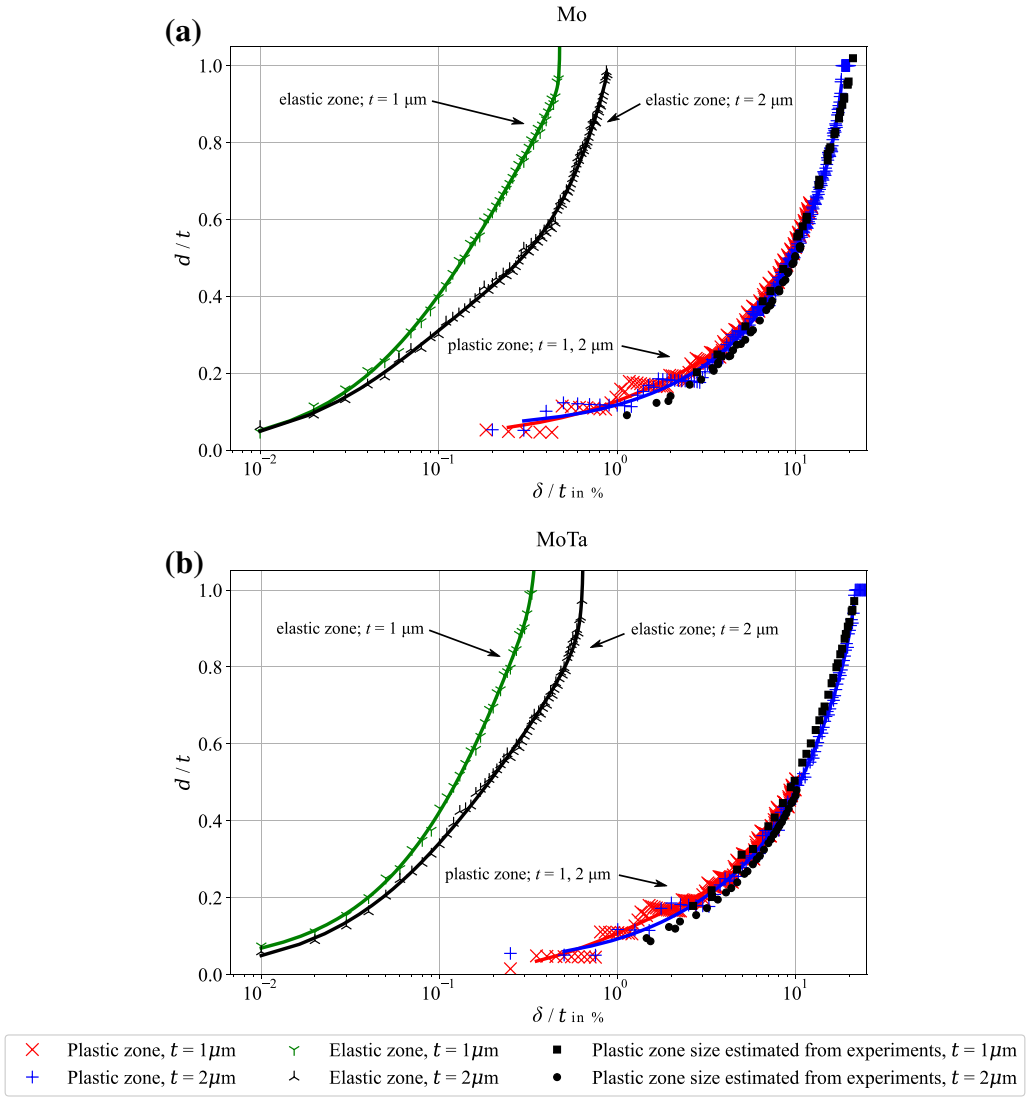


**Figure 6:** Extent of the elastically and plastically deformed volume during nanoindentation as a function of the indentation depth (normalized to the film thickness), numerical results complemented by the plastic zone size estimated from the experiments by Eq. (1), (a) represents the results for Mo thin films and (b) represents the results for MoTa thin films.

between the short and long range zones (see Figs. 1 and 5). Subsequently, from the interface the elastic zone grows to the substrate and the deformed volume of the substrate is much larger than that of thin film [while at the same strain levels, see Fig. 5(b)] resulting in severe substrate deformation and bending of the thin film. The actual extent and speed of the elastic zone growth in the film/substrate is not largely dependent on the film's Young's modulus, since the difference between Mo and MoTa films elastic properties is rather significant, but the elastic zone growth is similar. From the FE models, a general conclusion can be found that for metallic thin films, the elastic deformation reaches the substrate much faster than it was expected with the (inadequate) use of the "10% rule of thumb" for measuring *E*. It can be argued that a minimal film thickness of 5 µm will lead to usefulness of the 10% rule. This argument is further solidified by the fact that for 2 µm films the elastic zone growth is (in relation to the film thickness) slightly slower than for 1 µm films.

For a visualization of the stress–strain fields when the cross-sectional indentation is performed, the elastically and plastically deformed zones were extracted from the cross-sectional indentation FE simulation (for films on Si substrate embedded in the resin). Results in Fig. 7 clearly shows an influence of the indents spanning through the substrate and embedding resin. Figure 7(a) illustrates that both substrate and resin are subjected to displacement between 5 and 13 nm in a significant volume whereas in Fig. 7(b) one can clearly see that the plastic zone starts to extend into the resin even for 100 nm indentation

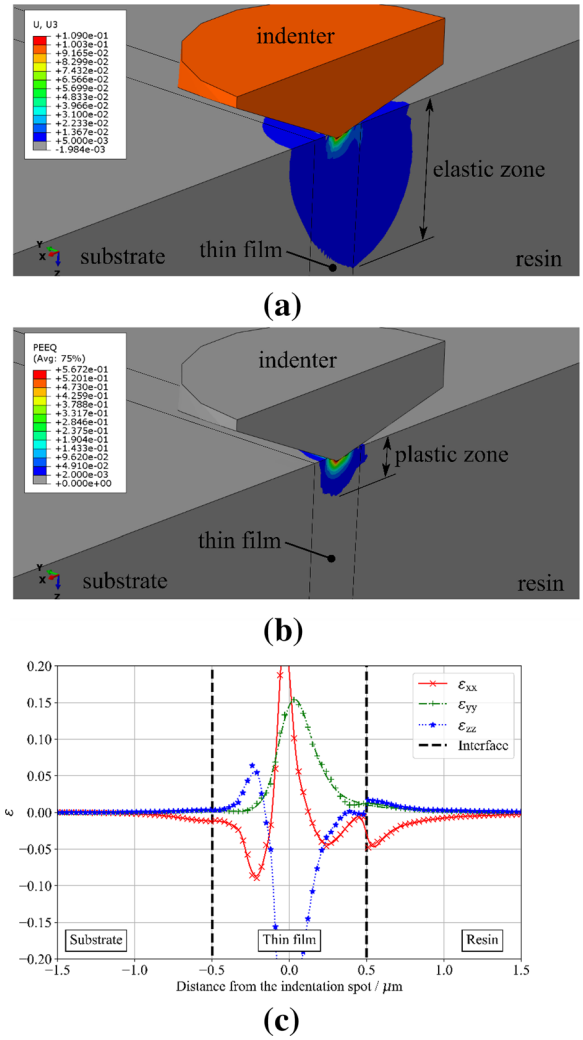


**Figure 7:** Example of the numerical results for CS indentation simulation, Mo thin film, $t = 1$ μm, $\delta = 100$ nm: a) displacement in the direction of indentation, indicating the elastically deformed volume, b) equivalent (von-Mises) plastic strain (PEEQ), indicating the plastically deformed volume and c) elastic strain components along the line on the surface of the specimen lying perpendicular to film-substrate and film-resin interfaces (denoted by the black dashed lines in the figure).

depth. This is in a good correlation with the obtained data (Fig. 3). According to previous measurements (see Fig. 6) and Eq. (1), the plastic zone radius is approximately 550 nm for the 1 μm thick Mo film and an indentation depth of 100 nm. When the CS indentation assumes the indentation point exactly at the centerline of the film thickness, there is a distance of 500 nm on both sides between the indenter tip and Si-Mo or Mo-resin interface. This means that a plastic zone that reaches the interface with the Si substrate and with the resin for the indentation depth of 10% of the film thickness is expected. While this phenomenon is demonstrated on the 1 μm thick Mo film, it is valid for both modeled materials and film thicknesses and a strong reason why lower $H$ values were measured.

While the largest strain values are located understandably directly under the indenter, the elastic deformation spans outside of the thin film [see the detailed elastic strain plots in Fig. 7(c)]. The strain component $\varepsilon_{xx}$ exhibits the compressive deformation in both the substrate and resin, where it reaches a value of 0.05 and the strain component $\varepsilon_{zz}$ shows small (but not negligible) tensile deformation in the resin. The observed elastic deformation in the resin has a radius larger than one-half of the film thickness. The extent of elastic and plastic deformation into the substrate and embedding material during a shallow CS indentation is in a good agreement with experimental CS measurements (see Fig. 3) and strongly underestimated values of $H$ and $E$ were observed. It has to be noted that the simulations of both thin film materials and both thicknesses show the same trends. Combined, the experimental CS indentation and simulations show that the CS indentation for very small samples embedded in soft materials is not usable, even if the exact centerline of the film is indented.

## Recommended nanoindentation procedure

According to presented results, several key-points can be extracted and formulated into a set of recommendations to measure the mechanical behavior of thin films using nanoindentation. These include sample preparation, suggested indentation procedure and results processing. If additional FE analysis is available, it could be used to validate experiments.

Thick films, generally greater than 2 μm, on rigid substrates (silicon, MgO, Alumina) are ideal film/substrate systems for nanoindentation. More compliant substrates will exaggerate the underestimation of the film's mechanical behavior. Film surfaces should be as smooth as possible for used application or the surface roughness has to be known prior the nanoindentation. Cross-sectional indentation is not recommended, however, if there is a need for using it, it is recommended that the sample be embedded in stiff materials. In general, one should avoid compliant substrates, such as polymers.

For indentation experiments, dynamic or quasi-static indentation can be used as long as many indents are performed to have enough statistics (approximately 50 to 100 indents, more is always better). The whole load range of the indenter should be used to identify indentation zones (see Fig. 2). If possible, very small indentation depths should be used, while keeping the machine and area function resolution in mind. It is imperative that indents be performed in both the thin film and substrate (and embedding material if used) to enable separation of substrate and film material properties. Without knowledge of the substrate, indented at the same time with the same tip and indenter conditions, proper comparisons cannot be made. Use as sharp an indentation tip as possible. A sharper tip contributes to the localization of elastic deformation; thus, it propagates

much slower towards the film–substrate interface [28]. This is in good agreement with the studies of [50, 51] where the tip radius was found to influence the CRTD. At a minimum, evaluate the tip radius before starting and ensure the tip is well calibrated.

The obtained $P$–$\delta$ curves can be analyzed with the O–P method, J–O method or any other suitable method to measure the hardness or elastic modulus of the film and substrate. Comparison between the film and substrate results is necessary as well as plotting the hardness and elastic values as a function of $h_c/t$. From the appropriate plots, the indentation Zones (according to Fig. 2) can be identified. For hardness measurements, it is best to use the Plateau Zone H3 to interpret film hardness. To estimate the elastic modulus, either a polynomial fit of sufficient amount of data points (hence, a large number of indents has to be made at the near surface of the film) can be used and extrapolated to $\delta/t = 0$. If there is a large number of small-depth indents (less than 2–3% of the film thickness) with a small scatter and exhibiting a plateau region (different than the substrate) in the Film-affected Zone E1, the mean value can be used to estimate the elastic modulus. However, the take home message is that the "10% rule of thumb" can only be used for thin film hardness measurements while a sufficient amount of indents has to be performed in a wide range of contact depths $h_c$. A different approach or a very thick film (approximately 5 μm thick) should be used to measure thin film elastic modulus with nanoindentation.

## Conclusions

Nanoindentation to various contact depths was performed on known material systems (Mo and MoTa thin films on Si substrate) and the resulting dependencies of film hardness and elastic modulus were compared with the known values and correlated with numerical simulations of the indentation process. Using the plastic and elastic zone as a definition for the usability of the experimental data can be seen as an improvement to the former criteria solely based on the deviations from bulk load–displacement curves. This allows not only the separation of the critical depth for elastic modulus and hardness, but it is also expected to allow calibration of new rules for the CRTD in a more physical way. While the hardness measurement of thin films systems with similar properties can be performed for indentation depths around 10% or greater of the film thickness, the extent of the elastic zone under the tip into the substrate does not allow for the elastic modulus to be easily measured. Therefore, for any elastic modulus measurement of thin films using nanoindentation, a large set of indents should be generated for both the film and substrate ranging from small indentation depths (less than 1% of the film thickness) to more than 10% of the film thickness to get the actual dependence of the elastic modulus on the contact depth and the possibility to remove the substrate influence. Additionally, very thick films and sharp indenter tips are suggested to improve the measurements further. The circumvention of the substrate effects (and, therefore, the whole 10% rule) by cross-sectional nanoindentation is not recommended since presented results show large deviation of $E$ and $H$ when such method is used. With use of proper methodology, the presented indentations measured $E_{Mo} = 316$ GPa (with use of J-O method and approximation of $h_c/t = 0$), $H_{Mo} = 11.8 \pm 1.33$ GPa, $E_{MoTa} = 260$ GPa and 246 GPa (with use of O–P and J-O methods, respectively, both with approximation of $h_c/t = 0$) and $H_{MoTa} = 14.1 \pm 0.17$ GPa. These values are in a good agreement with the expected values for Mo and MoTa materials. An exception was found when using the O–P method for the Mo films measured where a much lower than expected elastic modulus value ($E_{Mo,O-P} = 276$ GPa) was measured. The lower modulus was most likely influenced by the very high surface roughness observed for the Mo films. Finally, the 10% rule of thumb is not an adequate way to measure the film-only mechanical properties and it should be avoided.

## Methods

### Materials

The Mo and MoTa films studied in the current work were deposited onto (100) silicon substrates (dimensions $6 \times 20$ mm$^2$, thickness 325 μm) using a laboratory scale direct current (d.c.) magnetron sputter system. Three circular planar targets (Mo and Ta targets with a diameter of 50.8 mm and a thickness of 6 mm each, provided by Kurt J. Lesker (Ta—purity 99.95%) and Plansee SE (Mo—purity 99.97%) were fixed to unbalanced AJAA320-XP magnetrons and focused onto the center of a rotatable sample holder at a distance of 40 mm. Prior to deposition, the substrates were ultrasonically cleaned in ethanol for 300 s and dried in hot air. The substrates were mounted onto the rotatable substrate holder (kept on a floating potential) with Kapton tape. The base pressure of the sputter system was always less than $1 \times 10^{-3}$ Pa. The substrates were plasma cleaned at an Ar pressure of 1 Pa in an asymmetrically bipolar pulsed d.c. plasma using a substrate voltage of − 350 V and a frequency of 50 kHz for 120 s. Two film thicknesses, namely 1 and 2 μm, Mo and MoTa alloy films were deposited without external heating with constant discharge powers of 188 W for the Mo and 130 W for the Ta magnetron at an Ar pressure of 0.25 Pa. With these discharge powers, deposition times of 1720 and 3440 s for 1 and 2 μm thick Mo films were used. For MoTa alloys, deposition times of 866 and 1732s were used for the 1 and 2 μm film thicknesses, respectively. The same deposition conditions were used for MoTa alloy interlayers in [59]. As shown in an earlier work, the chosen composition Mo50Ta50 yields a solid solution [60], this is also backed-up by AFLOW-CHULL, a cloud-oriented platform for autonomous phase stability analysis where

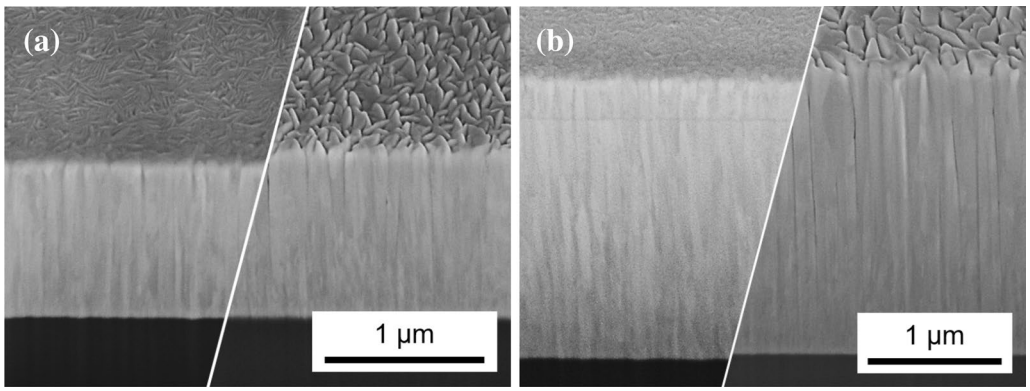


**Figure 8:** FIB-SEM images of the thin films (surface and cross-section): (a) 1 µm thickness: MoTa (left)—Mo (right), (b) 2 µm thickness: MoTa (left)—Mo (right).

it is shown to be thermodynamic stable [61]. Since no external heating was applied, the substrate temperature did not rise above 50 °C during deposition. Energy dispersive X-ray (EDX) spectroscopy, equipped on a scanning electron microscopy (SEM, Leo1525, Zeiss) with ZAF corrections yielded a 49.7 ± 3.8 at.% Mo composition of the MoTa alloy films. The ZAF correction corrects inter-element effects in a material, where Z is the correction of the atomic number, A for absorption effects and F for fluorescence.

Information on the film thicknesses was accessible via cross-sectional cuts using a focused ion beam (FIB, Zeiss LEO1540) with Gallium ions for the milling. The thickness was then determined from inspection of the cross sections with SEM on the same instrument. The exact respective film thicknesses of the 1 µm and 2 µm thick Mo films are 1040 and 2130 nm. The exact respective film thicknesses of the 1 µm and 2 µm thick MoTa alloy films are 960 and 1900 nm [see Fig. 8(a) and (b)]. The surface roughness was determined with a Dimension Icon atomic force microscope (Bruker) in tapping mode. For the 1 µm and 2 µm thick Mo films, RMS-roughness of 20 ± 1 nm and 37 ± 1 nm were respectively determined. For the 1 µm and 2 µm thick MoTa alloy films, RMS-roughness of 2 ± 0.1 nm and 3 ± 1 nm were respectively determined.

## Experiments

Nanoindentation was performed on a TS77 Select from Bruker-Hysitron using a well-calibrated Berkovich tip. Before indenting, the tip was imaged with confocal laser scanning microscopy (CLSM–Olympus 4100 OLS) and self-imaging (SI) over a TGT1 silicon spike grid from NT-MDT. From these images the tip radius was approximated to 300 nm [62]. The area function and frame compliance calibrations were made using 100 OL indents into fused silica with a 10 s load–10 s unload loading profile and maximum loads between 100 µN and 10 mN, resulting in the calibrated area function in range between 7 to 180 nm of $h_c$.

Quasi-static indents into the Mo and MoTa films as well as into the Si substrate were performed two ways: OL and DC. OL indents were made using the full load range (100 µN to 10 mN) with constant loading time (10 s), leading to similar maximal absolute contact depth for both film thicknesses capped by the maximal load usable with the TS77 setup. Therefore, two relative ranges of results were obtained whereas the effective relative contact depth (when divided by the film thickness) for the 2 µm film is half of the relative value for 1 µm film. DC indents were set to a maximum indentation depth of 10% of the film thickness (100 nm or 200 nm for 1 µm and 2 µm thick films, respectively). A total of 25 DC and 100 OL indents were made into each film in several subsequent indentation runs. Additionally, CS specimens were prepared where all films were indented parallel to the film surface to test if the CS indentation may solve the indentation depth issue. Films were embedded in a polymer resin, followed by grinding and polishing the surface to a 1 µm finish using colloidal silica. Nine DC indents were performed for each film type with the maximum indentation depth set to 10% of the film thickness. The indents were positioned in the center of the film by first scanning a large area with tip (scanning probe microscopy). In the Si substrate constant loading time (10 s) indents were performed (150 indents in total) on the top of its surface and nine indents in the CS. Additionally, nine indents in the embedding resin were performed.

All of the load–displacement curves were analyzed using the Oliver and Pharr (O–P) method [53] and the same area function. The elastic modulus, $E$, was evaluated from the reduced elastic modulus, $E_r$, values (2):

$$\frac{1}{E_r} = \frac{1-\nu_t^2}{E_t} + \frac{1-\nu^2}{E}, \tag{2}$$

where the tip Young's modulus, $E_t$, was 1170 GPa and its Poisson's ratio, $\nu_t = 0.17$, Poisson's ratio of the film, $\nu$, was different

for each material: Mo = 0.28, Si = 0.3, MoTa = 0.3. The area function was checked midway through the experiments and the tip was imaged again with the spikes (SI method) to check for any tip wear.

Moreover, the method by J–O [14] was used as an additional method for evaluation of the reduced Young's modulus $E_r$ directly from measured hardness, $H$ (obtained by standard, O–P procedure), indentation load, $P$, and slope of the unloading portion of the load–displacement curve, $S$, from relation (3):

$$\frac{H}{E_r^2} = \frac{4}{\pi} \cdot \frac{P}{S^2} \rightarrow E_r = \frac{S}{2}\sqrt{\frac{\pi \cdot H}{P}}. \quad (3)$$

This method allows one to avoid the introduction of errors due to change of the indenter tip shape when calculating the elastic modulus, because it does not use the indenter area (calibration) function. After finishing all indents, SI and CLSM images were made of the tip to determine if the tip shape changed due to indenting and to measure the tip radius. It was found that the tip radius changed from 300 to 500 nm after performing the indents using the same routine [62].

## Numerical model

To create and compute the numerical model of the indentation, the Abaqus code was used. Since the geometry of the Berkovich tip is not fully axisymmetric, a 3D model was used [Fig. 9(a)]. However, some symmetry planes were utilized to simplify the model and reduce the evaluation time. Only one sixth of the geometrical model is needed to represent the indentation process. The geometrical model itself consisted of the Berkovich tip with tip radius 300 nm (according to the real tip radius measured before and during the experiments, note that only the initial, sharp tip was considered to show the ideal experimental setup and the tip wear was not considered since it is not the aim of this study) and the specimen itself (thin Mo and MoTa film with 1 μm and 2 μm thicknesses for two different models, both on the thick Si substrate) as shown in Fig. 9(b).

The width of the specimen was 1 mm to have the boundaries of the model in a safe distance from the area of interest to avoid any unwanted interaction. The symmetrical boundary conditions were applied on actual symmetry planes—the displacement in the direction perpendicular to each symmetry plane on respective boundaries were fixed. The displacement of the indenter tip in the $z$-axis (third

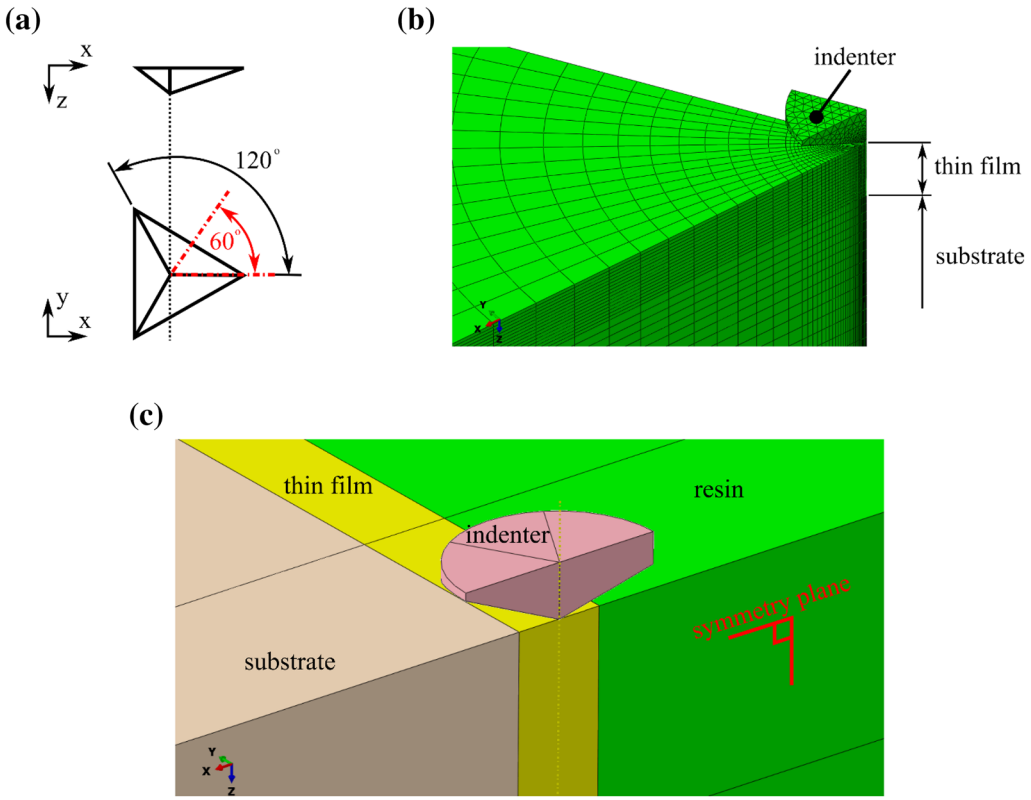


**Figure 9:** (a) Berkovich tip geometry (schema) with symmetry planes denoted by the red lines; (b) geometry and discretization of the FE model used for modeling the nanoindentation; (c) schematic view on the model of CS indentation with each layer denoted by its name and color, symmetry plane is parallel to global $x$–$z$ plane and the indentation direction is in the global $z$-direction.

**TABLE 1:** Material constants used in the FE model.

| | $E$ (GPa) | $\nu$ | $\sigma_y$ (GPa) |
|---|---|---|---|
| Indenter tip | 1170 | 0.17 | – |
| Si substrate | 170 | 0.3 | – |
| Mo film | 329 | 0.28 | 4 |
| MoTa film | 255 | 0.3 | 5.4 |

axis) was set to ramp from 0 nm to indentation depths corresponding to the range of displacements obtained in the experiment (either OL or DC) and back to 0 nm to model the unloading part of the load–displacement curve. To mimic the experimental procedure, the displacement of the bottom face of the substrate in the global model in the perpendicular direction was fixed. The frictionless contact was applied between the indenter tip and the free surface of the thin films, this is considered reasonable, since the friction coefficient is known to only have a marginal influence on the indentation curve [63–65] mainly the pile up and sink in behavior are effected by the choice in parameter [65]. In the modeling procedure several different material models were used. All of them were defined by the parameters shown in Table 1.

The indenter tip and the substrate were assumed to be linear elastic, defined only by the Young's modulus, $E$, and Poisson's ratio, $\nu$. Since the indentation can create a high increase in stress under the indenter tip, the elastic–plastic behavior of the Mo and MoTa films was assumed to cover the real material deformation under high loads. This material model was defined with the addition of the yield stress value (according to hardness measurements). For the sake of simplicity, the response of the material was assumed to be elastic—ideally plastic with no hardening.

Additionally, the CS indents were modeled to obtain the stress–strain fields around the indenter tip in the sample and its surroundings embedded in the soft resin. Since the asymmetrical CS specimen layout does not allow the use of sixfold rotational symmetry (as in the case of the surface indentation), the CS FE model had to be more complex. With a proper indenter tip rotation in relation to the specimen, one symmetry plane could be used (see Fig. 9c). The indentation was modeled always in the center of the thin film CS (as an ideal case). The maximum indentation depth in the FE model was set (according to experimental CS measurements) to 10% of the respective film thickness. The material properties of the thin film and substrate were the same as for the surface indentation model, however, the CS model was extended by the material model of the resin, which consisted of a Young's modulus of 4.5 GPa, a Poisson's ratio of 0.35 and the yield stress of 115 MPa.

## Acknowledgments

V.L. Terziyska and C. Mitterer from the Department of Materials Science of the Montanuniversität Leoben are gratefully acknowledged for depositing the films used in this work.

## Author contributions

All authors contributed to the study conception and design. Material preparation was performed by PK and MJC, data collection and analysis were performed by SZ, COWT, MJC and PK and the numerical modeling and representation of the models and results was performed by SZ. The first draft of the manuscript was written by SZ and MJC. All authors commented on previous versions of the manuscript, read and approved the final manuscript.

## Funding

Open access funding provided by Österreichische Akademie der Wissenschaften.

## Data availability

The datasets generated during and/or analyzed during the current study are available from the corresponding author on reasonable request.

## Code availability

The input files (codes) from Abaqus software used during the current study are available from the corresponding author on reasonable request.

## Declarations

**Conflict of interest** The authors have no competing interests to declare that are relevant to the content of this article.

## References

1. W.D. Nix, Mechanical properties of thin films. Metall. Trans. A. **20A**, 2217–2245 (1989). https://doi.org/10.1146/annurev.ms.20.080190.002135
2. H. Bückle, Use of hardness test to determine other material properties, in *The Science of Hardness Testing and Its Research Applications*. ed. by J.H. Westbrook, H. Conrad (American Society for Metals, Metals Park, OH, 1973), pp. 453–494
3. D. Tabor, *Hardness of Metals* (Clarendon Press, Oxford, 1951)
4. J.R. Cahoon, W.H. Broughton, A.R. Kutzak, The determination of yield strength from hardness measurements. Metall. Trans. **2**, 1979–1983 (1971). https://doi.org/10.1007/BF02913433
5. Z.H. Xu, D. Rowcliffe, Finite element analysis of substrate effects on indentation behaviour of thin films. Thin Solid Films **447–448**, 399–405 (2004). https://doi.org/10.1016/S0040-6090(03)01071-X
6. S.J. Bull, Microstructure and indentation response of TiN coatings: The effect of measurement method. Thin Solid Films **688**, 137452 (2019). https://doi.org/10.1016/j.tsf.2019.137452
7. A.M. Korsunsky, M.R. McGurk, S.J. Bull, T.F. Page, On the hardness of coated systems. Surf. Coatings Technol. **99**, 171–183 (1998). https://doi.org/10.1016/S0257-8972(97)00522-7
8. P.J. Burnett, D.S. Rickerby, The relationship between hardness and scratch adhesion. Thin Solid Films **154**, 403–416 (1987)
9. T.Y. Tsui, G.M. Pharr, Substrate effects on nanoindentation mechanical property measurement of soft films on hard substrates. J. Mater. Res. **14**, 292–301 (1999). https://doi.org/10.1557/JMR.1999.0042
10. R. Saha, W.D. Nix, Effects of the substrate on the determination of thin film mechanical properties by nanoindentation. Acta Mater. **50**, 23–38 (2002). https://doi.org/10.1016/S1359-6454(01)00328-7
11. J. Chen, S.J. Bull, On the relationship between plastic zone radius and maximum depth during nanoindentation. Surf. Coat. Technol. **201**, 4289–4293 (2006). https://doi.org/10.1016/j.surfcoat.2006.08.099
12. H. Li, J.J. Vlassak, Determining the elastic modulus and hardness of an ultra-thin film on a substrate using nanoindentation. J. Mater. Res. **24**, 1114–1126 (2009)
13. R. Saha, W.D. Nix, Soft films on hard substrates — nanoindentation of tungsten films on sapphire substrates. Mater. Sci. Eng. A. **321**, 898–901 (2001)
14. D.L. Joslin, W.C. Oliver, A new method for analyzing data from continuous depth-sensing microindentation tests. J. Mater. Res. **5**, 123–126 (1990). https://doi.org/10.1557/JMR.1990.0123
15. W.D. Nix, Elastic and plastic properties of thin films on substrates: nanoindentation techniques. Mater. Sci. Eng. A. **A234–236**, 37–44 (1997). https://doi.org/10.1016/s0921-5093(97)00176-7
16. W.D. Nix, Metallic thin films: stresses and mechanical properties. Met. Film. Electron. Opt. Magn. Appl. Struct. Process. Prop. (2014). https://doi.org/10.1533/9780857096296.2.353
17. I.N. Sneddon, The relation between load and penetration in the axisymmetric Boussinesq problem for a punch of arbitrary profile. Int. J. Eng. Sci. **3**, 47–57 (1965). https://doi.org/10.1016/0020-7225(65)90019-4
18. R. Saha, Z. Xue, Y. Huang, W.D. Nix, Indentation of a soft metal film on a hard substrate: strain gradient hardening effects. J. Mech. Phys. Solids. **49**, 1997–2014 (2001). https://doi.org/10.1016/S0022-5096(01)00035-7
19. H.Y. Yu, S.C. Sanday, B.B. Rath, The effect of substrate on the elastic properties of films determined by the indentation test—axisymmetric Boussinesq problem. J. Mech. Phys. Solids **38**, 745–764 (1990). https://doi.org/10.1016/0022-5096(90)90038-6
20. A.C. Fischer-Cripps, *Nanoindentation*, 2nd edn. (Springer, New York, 2004)
21. S.M. Han, R. Saha, W.D. Nix, Determining hardness of thin films in elastically mismatched film-on-substrate systems using nanoindentation. Acta Mater. **54**, 1571–1581 (2006). https://doi.org/10.1016/j.actamat.2005.11.026
22. M.J. Cordill, N.R. Moody, W.W. Gerberich, Effects of dynamic indentation on the mechanical response of materials. J. Mater. Res. **23**, 1604–1613 (2008). https://doi.org/10.1557/JMR.2008.0205
23. K.W. Siu, A.H.W. Ngan, Oscillation-induced softening in copper and molybdenum from nano- to micro-length scales. Mater. Sci. Eng. A. **572**, 56–64 (2013). https://doi.org/10.1016/j.msea.2013.02.037
24. K. Durst, B. Backes, O. Franke, M. Göken, Indentation size effect in metallic materials: modeling strength from pop-in to macroscopic hardness using geometrically necessary dislocations. Acta Mater. **54**, 2547–2555 (2006). https://doi.org/10.1016/j.actamat.2006.01.036
25. A. Leitner, V. Maier-Kiener, D. Kiener, Dynamic nanoindentation testing: is there an influence on a material's hardness? Mater. Res. Lett. **5**, 486–493 (2017). https://doi.org/10.1080/21663831.2017.1331384
26. A.K. Nair, M.J. Cordill, D. Farkas, W.W. Gerberich, Nanoindentation of thin films: simulations and experiments. J. Mater. Res. **24**, 1135–1141 (2009). https://doi.org/10.1557/jmr.2009.0136
27. M.J. Cordill, M.S. Lund, J. Parker, C. Leighton, A.K. Nair, D. Farkas, N.R. Moody, W.W. Gerberich, The Nano-Jackhammer effect in probing near-surface mechanical properties. Int. J. Plasticity **25**, 2045–2058 (2009). https://doi.org/10.1016/j.ijplas.2008.12.015

28. F. Lofaj, D. Németh, The effects of tip sharpness and coating thickness on nanoindentation measurements in hard coatings on softer substrates by FEM. Thin Solid Films **644**, 173–181 (2017). https://doi.org/10.1016/j.tsf.2017.09.051
29. N.I. Tymiak, D.E. Kramer, D.F. Bahr, T.J. Wyrobek, W.W. Gerberich, Plastic strain and strain gradients at very small indentation depths. Acta Mater. **49**, 1021–1034 (2001). https://doi.org/10.1016/S1359-6454(00)00378-5
30. D. Kramer, H. Huang, M. Kriese, J. Robach, J. Nelson, A. Wright, D. Bahr, W.W. Gerberich, Yield strength predictions from the plastic zone around nanocontacts. Acta Mater. **47**, 333–343 (1998). https://doi.org/10.1016/S1359-6454(98)00301-2
31. R.K. Abu Al-Rub, G.Z. Voyiadjis, Analytical and experimental determination of the material intrinsic length scale of strain gradient plasticity theory from micro- and nano-indentation experiments. Int. J. Plasticity **20**, 1139–1182 (2004). https://doi.org/10.1016/j.ijplas.2003.10.007
32. K. Durst, B. Backes, M. Göken, Indentation size effect in metallic materials: correcting for the size of the plastic zone. Scr. Mater. **52**, 1093–1097 (2005). https://doi.org/10.1016/j.scriptamat.2005.02.009
33. G. Feng, W.D. Nix, Indentation size effect in MgO. Scr. Mater. **51**, 599–603 (2004). https://doi.org/10.1016/j.scriptamat.2004.05.034
34. W.D. Nix, H.J. Gao, Indentation size effects in crystalline materials: a law for strain gradient plasticity. J. Mech. Phys. Solids **46**, 411–425 (1998). https://doi.org/10.1016/s0022-5096(97)00086-0
35. M.J. Cordill, D.M. Hallman, N.R. Moody, D.P. Adams, W.W. Gerberich, Thickness effects on the plasticity of gold films. Metall. Mater. Trans. A Phys. Metall. Mater. Sci. **38A**, 2154–2159 (2007). https://doi.org/10.1007/s11661-006-9011-7
36. R.D. Mindlin, A review of the photoelastic method of stress analysis. I. J. Appl. Phys. **10**, 222–241 (1939). https://doi.org/10.1063/1.1707300
37. J.F. Orr, J.B. Finlay, Photoelastic stress analysis, in *Optical Measurement Methods in Biomechanics* (Springer, Boston, 1997). https://doi.org/10.1007/978-0-585-35228-2_1.
38. J.S. Hawong, J.H. Nam, K.H. Kim, O.S. Kwon, G. Kwon, S.H. Park, A study on the development of photoelastic experimental hybrid method for colour isochromatics (I). J. Mech. Sci. Technol. **24**, 1279–1287 (2010). https://doi.org/10.1007/s12206-010-0337-0
39. C. Niezrecki, P. Avitabile, C. Warren, P. Pingle, M. Helfrick, A review of digital image correlation applied to structural dynamics. AIP Conf. Proc. **1253**, 219–232 (2010). https://doi.org/10.1063/1.3455461
40. A. Weidner, H. Biermann, Review on strain localization phenomena studied by high-resolution digital image correlation. Adv. Eng. Mater. (2021). https://doi.org/10.1002/adem.202001409
41. R. Janeliukstis, X. Chen, Review of digital image correlation application to large-scale composite structure testing. Compos. Struct. **271**, 114143 (2021). https://doi.org/10.1016/j.compstruct.2021.114143
42. A. Zeilinger, J. Todt, C. Krywka, M. Müller, W. Ecker, B. Sartory, M. Meindlhumer, M. Stefenelli, R. Daniel, C. Mitterer, J. Keckes, In-situ observation of cross-sectional microstructural changes and stress distributions in fracturing TiN thin film during nanoindentation. Sci. Rep. **6**, 22670 (2016). https://doi.org/10.1038/srep22670
43. A.K. Bhattacharya, W.D. Nix, Finite element simulation of indentation experiments. Int. J. Solids Struct. **24**, 881–891 (1988). https://doi.org/10.1016/0020-7683(88)90039-X
44. A. Nasto, A. Ajdari, A. Lazarus, A. Vaziri, P.M. Reis, Localization of deformation in thin shells under indentation. Soft Matter **9**, 6796–6803 (2013). https://doi.org/10.1039/c3sm50279a
45. C. Shi, H. Zhao, H. Huang, L. Xu, L. Ren, M. Bai, J. Li, X. Hu, Effects of indenter tilt on nanoindentation results of fused silica: an investigation by finite element analysis. Mater. Trans. **54**, 958–963 (2013). https://doi.org/10.2320/matertrans.M2012400
46. S. Syngellakis, H. Habbab, B.G. Mellor, Finite element simulation of spherical indentation experiments. Int. J. Comput. Methods Exp. Meas. **6**, 749–763 (2018). https://doi.org/10.2495/CMEM-V6-N4-749-763
47. C. Gao, H. Proudhon, M. Liu, Three-dimensional finite element analysis of shallow indentation of rough strain-hardening surface. Friction. **7**, 587–602 (2019). https://doi.org/10.1007/s40544-018-0245-3
48. A.K. Bhattacharya, W.D. Nix, Analysis of elastic and plastic deformation associated with indentation testing of thin films on substrates. Int. J. Solids Struct. **24**, 1287–1298 (1988)
49. J. Chen, S.J. Bull, Loading rate effects on the fracture behaviour of solar control coatings during nanoindentation. Thin Solid Films **516**, 128–135 (2007). https://doi.org/10.1016/j.tsf.2007.08.131
50. Y. Sun, T. Bell, S. Zheng, Finite element analysis of the critical ratio of coating thickness to indentation depth for coating property measurements by nanoindentation. Thin Solid Films **258**, 198–204 (1995). https://doi.org/10.1016/0040-6090(94)06357-5
51. N. Panich, P. Wangyao, T. Chomtohsuwan, S. Yong, Finite element analysis of the critical ratio of coating thickness to indentation depth of soft coating on a harder substrate by nanoindentation. ScienceAsia **32**, 411–416 (2006). https://doi.org/10.2306/scienceasia513-1874.2006.32.411
52. E. Felder, S. Roy, E. Darque-Ceretti, Characterization of the adhesion of thin film by cross-sectional nanoindentation. Analysis of the substrate edge chipping and the film delamination. Compt. Rend. Mec. **339**, 443–457 (2011). https://doi.org/10.1016/j.crme.2011.05.003
53. W.C. Oliver, G.M. Pharr, An improved technique for determining hardness and elastic modulus using load and displacement

sensing indentation experiments. J. Mater. Res. **7**, 1564–1583 (1992). https://doi.org/10.1557/JMR.1992.1564

54. J.J. Hall, Electronic effects in the elastic constants of n-type silicon. Phys. Rev. **161**, 756–761 (1967). https://doi.org/10.1103/PhysRev.161.756
55. E.J. Boyd, D. Uttamchandani, Measurement of the anisotropy of Young's modulus in single-crystal silicon. J. Microelectromech. Syst. **21**, 243–249 (2012). https://doi.org/10.1109/JMEMS.2011.2174415
56. L. Zhang, R. Barrett, P. Cloetens, C. Detlefs, M. Sanchez Del Rio, Anisotropic elasticity of silicon and its application to the modelling of X-ray optics. J. Synchrotron Radiat. **21**, 507–517 (2014). https://doi.org/10.1107/S1600577514004962
57. S. Chen, L. Liu, T. Wang, Investigation of the mechanical properties of thin films by nanoindentation, considering the effects of thickness and different coating-substrate combinations. Surf. Coat. Technol. **191**, 25–32 (2005). https://doi.org/10.1016/j.surfcoat.2004.03.037
58. W.D. Callister, D.G. Rethwisch, *Materials Science and Engineering: An Introduction*, 8th edn. (Wiley, New York, 2010)
59. P. Kreiml, M. Rausch, V.L. Terziyska, H. Köstenbauer, J. Winkler, C. Mitterer, M.J. Cordill, Balancing the electromechanical and interfacial performance of Mo-based alloy films. Materialia (2020). https://doi.org/10.1016/j.mtla.2020.100774
60. A.M. Hofer, G. Mori, A. Fian, J. Winkler, C. Mitterer, Improvement of oxidation and corrosion resistance of Mo thin films by alloying with Ta. Thin Solid Films **599**, 1–6 (2016). https://doi.org/10.1016/j.tsf.2015.12.052
61. C. Oses, E. Gossett, D. Hicks, F. Rose, M.J. Mehl, E. Perim, I. Takeuchi, S. Sanvito, M. Scheffler, Y. Lederer, O. Levy, C. Toher, S. Curtarolo, AFLOW-CHULL: cloud-oriented platform for autonomous phase stability analysis. J. Chem. Inf. Model. **58**, 2477–2490 (2018). https://doi.org/10.1021/ACS.JCIM.8B00393/SUPPL_FILE/CI8B00393_SI_006.PDF
62. C. Saringer, M. Tkadletz, M. Kratzer, M.J. Cordill, Direct determination of the area function for nanoindentation experiments. J. Mater. Res. (2021). https://doi.org/10.1557/s43578-021-00113-9
63. J.L. Bucaille, S. Stauss, E. Felder, J. Michler, Determination of plastic properties of metals by instrumented indentation using different sharp indenters. Acta Mater. **51**, 1663–1678 (2003). https://doi.org/10.1016/S1359-6454(02)00568-2
64. X. Huang, A.A. Pelegri, Mechanical characterization of thin film materials with nanoindentation measurements and FE analysis. J. Compos. Mater. **40**, 1393–1407 (2006). https://doi.org/10.1177/0021998305059728
65. W.C. Guo, G. Rauchs, W.H. Zhang, J.P. Ponthot, Influence of friction in material characterization in microindentation measurement. J. Comput. Appl. Math. **234**, 2183–2192 (2010). https://doi.org/10.1016/j.cam.2009.08.072